G. Shatil and D. J. Smith**

Life Prediction and High-Strain Multiaxial Fatigue of an Engineering Component

REFERENCE Shatil, G. and Smith, D. J., **Life prediction and high-strain multiaxial fatigue of an engineering component**, *Multiaxial Fatigue and Design*, ESIS 21 (Edited by A. Pineau, G. Cailletaud, and T. C. Lindley) 1996, Mechanical Engineering Publications, London, pp. 499–511.

ABSTRACT Assessment of the performance of a light vehicle suspension arm is carried out by using a procedure developed to predict high-strain multiaxial fatigue life. The procedure combines multiaxial fatigue correlation theories and local strain estimation methods with experimental biaxial fatigue test results. Two sets of experimental data were used in the analysis: data from biaxial fatigue of hollow specimens and from uniaxial fatigue of solid specimens. Four strain parameters were utilized namely: the maximum strain, the maximum shear strain, the Brown–Miller and the Lohr–Ellison parameters. Finally, these strain parameters were evaluated from elastic–plastic plane stress and plane strain finite-element analysis results. Four combinations of the correlating parameters and test conditions were used to estimate the component life and are compared with experimental results. The combination of the Lohr–Ellison parameter and biaxial fatigue data yielded the most conservative prediction and conversely the combination of the maximum strain and the uniaxial data gave a non-conservative estimate. The Brown–Miller parameter and uniaxial fatigue results predicted lives between those two extremes. These sequences of lives were obtained from the four combinations, irrespective of the applied load, or whether plane-stress or plane-strain conditions were assumed.

1 Introduction

Conventional methods of low-cycle fatigue (LCF) assessment of service components often use the local strain approach (1). A fundamental assumption for this approach is the similarity between the fatigue response at the critical location in the component (such as at a notch root) and the fatigue response of smooth specimens subject to uniaxial loading. However, many engineering parts are frequently subjected to multiaxial cyclic loading (2). A multiaxial state of stress or strain can also arise from sudden changes in geometry, such as in notches and fillets. Published work associated with the application of the local strain approach to multiaxial fatigue is typically concerned with multiaxial fatigue testing and correlation theories (3), estimation of notch stress and strain (4) and life assessment of service components (1, 5).

Extensions of the local approach to multiaxial fatigue often make use of multiaxial fatigue damage theories. Most studies in the low cycle multiaxial fatigue regime use a shear strain parameter to correlate different multiaxility conditions and to predict the number of cycles to crack initiation (6). Brown

*Department of Mechanical Engineering, University of Bristol, UK.

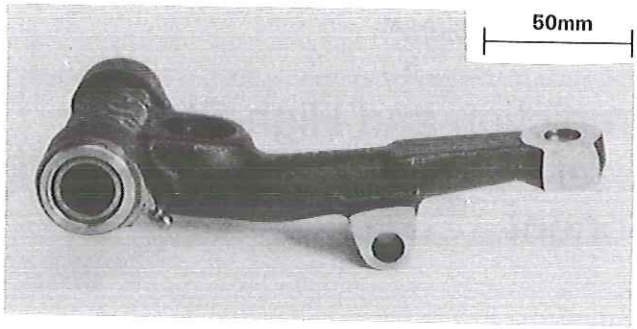

Fig 1 The Metro car suspension arm.

and Miller (7) developed a multiaxial fatigue failure theory employing the maximum shear strain parameter and a secondary tensile strain normal to the shear plane. The theory defined two cases. Case A for cracks propagating along the surface; and, Case B for cracks propagating inwards. For the more severe situation of Case B, Kandil et al. (8) suggest using the Tresca parameter. As an extension to the Brown–Miller model (7), Lohr and Ellison (9) developed a theory which applies the shear parameter acting on a through thickness plane as the correlating parameter in all cases. The Lohr–Ellison theory was applied to thin-walled specimen results where Case B dominated the fatigue life in most cases (9, 10).

Only a limited number of studies of the influence of geometry variation on predicting multiaxial fatigue damage development and life assessment of components (5, 11) have been carried out. Furthermore, life predictions using biaxial data tested under the full range of biaxiality ratios (Brown–Miller, Cases A and B cracks), do not appear to exist in the literature. Fash et al. (11) compared the fatigue damage process using thin-walled specimens and solid notched specimens in torsional loading where Case A cracks dominate the fatigue life. They show that the stress/strain gradient in the solid notched specimens constrained the development of cracks in the circumferential direction.

In the present work biaxial fatigue test results, multiaxial strain correlation parameters and finite-element elastic–plastic analyses were used to predict the fatigue life of a car suspension arm, Fig. 1. Estimated lives obtained from biaxial and uniaxial experimental results of thin-walled hollow specimens (10) and solid smooth specimens (12) respectively, are compared with the component fatigue lives.

2 Experiments and Results

Low-cycle fatigue (LCF) biaxial data for the suspension arm EN15R (BS150 M36) material were obtained from thin-walled specimens subject to internal

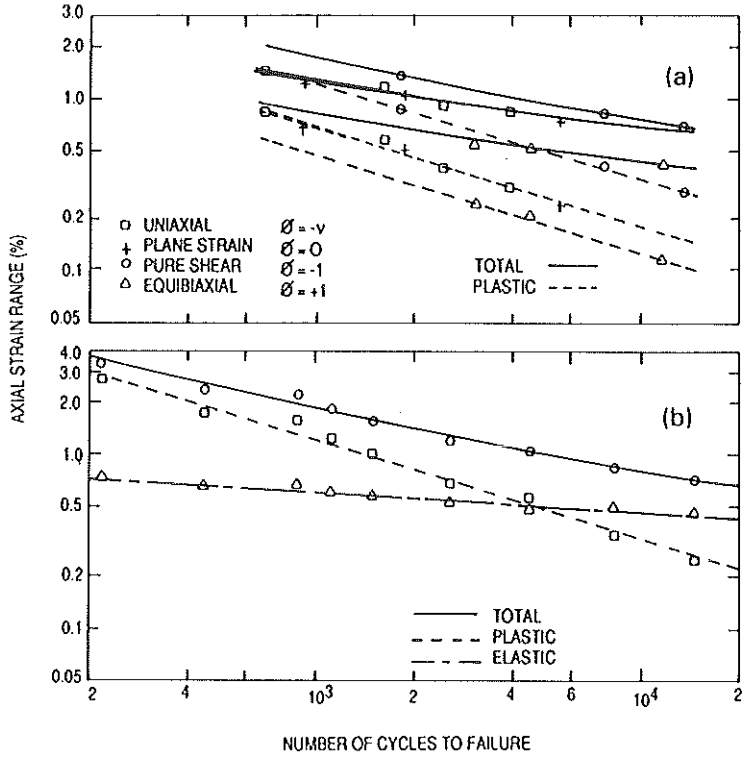

Fig 2 Fatigue results: (a) biaxial hollow specimens; (b) uniaxial solid specimens.

and external cyclic pressure and cyclic axial load. The chemical composition of the EN15R material was (%wt): 0.4C, 0.29Si, 1.47Mn, 0.019P and 0.004S. Young's modulus at room temperature was 205 GPa and the 0.2 percent proof stress was 438 MPa. The specimens were tested under four different ratios of diametral to axial surface strains, ϕ, namely -1, $-\nu$, 0 and $+1$, representing the full range of biaxiality ratios. Details of the experimental results are given elsewhere (**10**). Uniaxial tests were also conducted, using solid hourglass specimens (**12**) to obtain the material cyclic behaviour and LCF lives for a range of strain amplitudes. All experimental work was performed under constant amplitude strain control using servo-hydraulic test machines. The fatigue response of the specimens are shown in Fig. 2 in terms of the applied axial strain range as a function of the fatigue life. For pure shear tests with $\phi = -1$, the axial strain range was equal to minus the diametral strain range.

Car suspension arms (Fig. 1) were subject to constant bending load control amplitudes at much higher loads than for service conditions (**13**). The tests were a simplification of the random complex loading system which exists in the

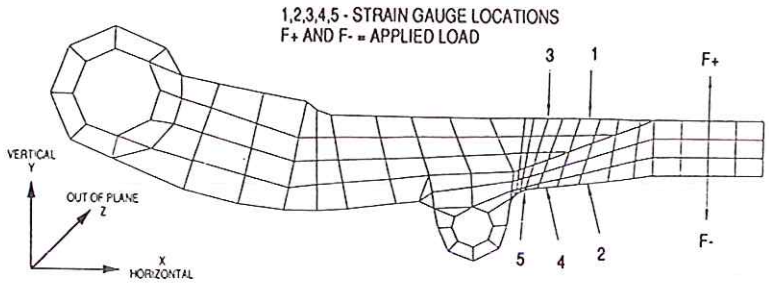

Fig 3 Finite-element mesh, strain gauge locations and applied load.

service condition. Each arm was constrained in the fatigue test through two bearings, labelled LB and MB in Fig. 1, lying in the outer plane axis (z). A uniaxial load was applied along the y-axis to the right bearing (RB). The constraints resulted in a bending moment about the z-axis.

The loading arrangement induced a significant stress concentration region during the fatigue tests near the boss, MB in Fig. 1. In this area localized plasticity was identified, leading to the development of fatigue cracks. Initial elastic measurements were carried out at a load range of ± 3 kN to determine the elastic stress response using strain gauges fixed to the suspension arm. The strain gauge locations are shown in Fig. 3. An axial (x) stress concentration factor of about 1.95 between the 'critical' site at location 5 and the 'normal' stress at location 1 was measured. A similar concentration factor (1.86) was obtained using photoelasticity analysis (**13**). Additional strain gauge measurements at the critical location were conducted along the out-of-plane (z) direction.

Two load ranges were examined; six fatigue tests were carried out under a load range of ± 14.8 kN and seven tests were conducted under a load range of ± 8.8 kN. For a given load range the cycles to failure from test to test varied significantly, with a factor of about two on life for the ± 14.8 kN range and a factor of about ten on life for the ± 8.8 kN tests.

3 Finite-Element Simulations

A two-dimensional model of the suspension arm was constructed, Fig. 3, using a finer mesh in the critical area. The left bearing (LB) was radially constrained, allowing rotation about the z-axis, and the middle boss (MB) was fully constrained assuming high friction force. Vertical load was applied to a line of nodes in the y-direction at the right bearing (RB) as shown in Fig. 3. Two boundary conditions were examined: plane-stress together with an approximation of the out-of-plane thickness variation; and, plane-strain with a uniform thickness.

An assessment of the accuracy of the finite-element models was carried out at the same load range (± 3 kN) as the elastic experimental test. The strains from the finite-element analysis were obtained from the approximate locations of the strain gauges (Fig. 3) for plane-stress and plane-strain conditions. The simulated stress concentration factor was 2.25 using the plane-stress model and 1.88 using the plane-strain model, compared to the measured concentration factor of approximately 1.95.

For the plane-stress analysis the stress ranges at locations 1 to 3 were about 10% less than the strain gauge measurements, while close to the critical area at locations 4 and 5, predicted strains were about 2% higher than the measured strains. In the plane-strain analysis the strain ranges at all locations were within $\pm 5\%$ of the experimental results. In both plane-stress and plane-strain analysis the maximum predicted strains approximately coincide with the location of the strain gauge exhibiting the maximum measured strains.

The uniaxial cyclic elastic–plastic stress–strain relationships (**12**) obtained from solid hourglass specimens, were used as input to the finite-element simulations. Analyses were performed assuming plane-stress or plane-strain conditions at the two experimental cyclic load levels (± 8.8 kN and ± 14.8 kN) and the cyclic elastic–plastic multiaxial strain ranges obtained at the critical location were subsequently used in a life prediction assessment described below.

4 Life Prediction Assessment Procedure

A general procedure which applies the biaxial fatigue data to predict the life of the service component subjected to constant amplitude, in-phase, multiaxial fatigue loading is shown schematically in Fig. 4. The procedure was carried out by first providing curves of equivalent strain parameter versus cycles to failure (master curves) from the biaxial or the uniaxial fatigue tests (**10**, **12**), and, secondly, computing lives from these master curves corresponding to the finite-element elastic–plastic simulated strains at the critical surface location (location 5, Figure 3). Four LCF strain-correlating parameters were used as follows.

4.1 *The maximum stress parameter*

Total maximum axial strain ranges were correlated to the LCF lives using the tradional Coffin–Manson and Basquin equations, where the total strain range $\Delta\varepsilon^{t}$ is given as the sum of the elastic and plastic strain ranges, $\Delta\varepsilon^{e}$ and $\Delta\varepsilon^{p}$ respectively so that

$$\Delta\varepsilon_x^t = \Delta\varepsilon_x^e + \Delta\varepsilon_x^p = AN_f^{-\alpha} + BN_f^{-\beta} \tag{1}$$

where $\Delta\varepsilon_x$ is the longitudinal strain for the solid and hollow specimens and the axial strain for the suspension arm. A, B, α and β are material constants.

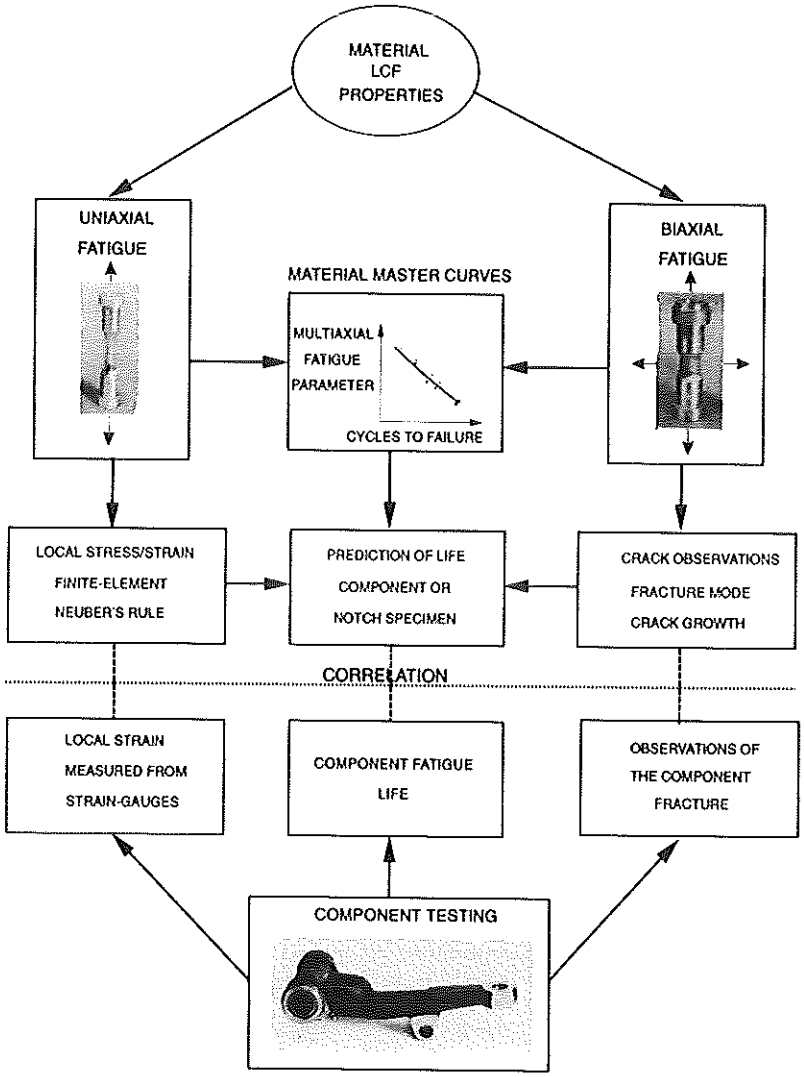

Fig 4 LCF constant amplitude life prediction procedure.

4.2 *The Brown–Miller strain parameter*

$$\Delta\varepsilon_{eq}^{t} = \left[\frac{\gamma_{max}}{2} + 0.2\varepsilon_n\right]^{e} + \left[\frac{\gamma_{max}}{2} + C\varepsilon_n\right]^{p} = AN_f^{-\alpha} + BN_f^{-\beta} \tag{2}$$

where

$$\frac{\gamma_{max}}{2} = \frac{\varepsilon_{max} - \varepsilon_{min}}{2} \quad \text{and} \quad \varepsilon_n = \frac{\varepsilon_{max} + \varepsilon_{min}}{2}$$

4.3 *The Lohr–Ellison parameter*

$$\Delta\varepsilon_{eq}^{t} = \left[\frac{\gamma^*}{2} + 0.2\varepsilon_n^*\right]^{e} + \left[\frac{\gamma^*}{2} + C\varepsilon_n^*\right]^{p} = AN_f^{-\alpha} + BN_f^{-\beta} \tag{3}$$

where

$$\frac{\gamma^*}{2} = \frac{\varepsilon_x - \varepsilon_y}{2} \text{ and } \varepsilon_n^* = \frac{\varepsilon_x + \varepsilon_y}{2} \text{ for the suspension arm}$$

and

$$\frac{\gamma^*}{2} = \frac{\varepsilon_z - \varepsilon_r}{2} \quad \text{and} \quad \frac{\varepsilon_z + \varepsilon_r}{2} \quad \text{for the thin-walled specimens}$$

4.4 *The maximum shear strain parameter*

$$\Delta\varepsilon_{eq}^{t} = \left[\frac{\gamma_{max}}{2}\right]^{e} + \left[\frac{\gamma_{max}}{2}\right]^{p} = AN_f^{-\alpha} + BN_f^{-\beta} \tag{4}$$

where

$$\frac{\gamma_{max}}{2} = \frac{\varepsilon_{max} - \varepsilon_{min}}{2}$$

The material constant C in equations 2 and 3 was assumed to be 0.2 since this was shown to correlate well with earlier results (**9**, **10**). An iterative technique was required to obtain, for each equation, the fatigue life corresponding to the simulated equivalent plastic and elastic strain ranges. Equations (1) and (2) were used to evaluate master curves employing data from the fatigue tests of the uniaxial solid specimens, while equations (3) and (4) were used with data from the biaxial thin-walled specimens.

The Brown–Miller parameter was evaluated for the uniaxial solid bar specimens by assuming that $\varepsilon_r = -\nu\varepsilon_z$ and substituting separately for elastic and plastic components, using $-\nu_e = 0.3$ and $-\nu_p = 0.5$ where ν_e and ν_p are elastic and plastic Poisson's ratios respectively. Insertion of these assumptions into equation (**2**) give

$$\frac{\gamma_{max}}{2} + 0.2\varepsilon_n = 0.72\Delta\varepsilon_x^e + 0.8\Delta\varepsilon_x^p \tag{5}$$

The maximum shear strain parameter was evaluated with the thin-walled specimens using the biaxiality conditions where Case B cracks dominate the fatigue lives (10), i.e. excluding the pure-shear data ($\phi = -1$).

Table 1 summarizes the combinations of the testing methods and the correlation theories and shows the constants used with each master curve to predict the car suspension arm fatigue life.

Table 1. Master curves used in the life prediction analysis

Strain parameter	Experimental method	Master curves constants			
		Elastic		Plastic	
		B	β	A	α
Maximum strain (ε_{max})	Uniaxial solid specimens	0.013	0.111	0.589	0.563
Maximum shear strain ($\gamma_{max}/2$, case B)	Biaxial hollow specimens	0.011	0.169	0.067	0.396
Brown–Miller ($\gamma_{max}/2 + 0.2\ \varepsilon_n$)	Uniaxial solid specimens	0.0082	0.111	0.373	0.563
Lohr–Ellison ($\gamma^*/2 + 0.2\varepsilon_n^*$)	Biaxial hollow specimens	0.0127	0.167	0.141	0.468

Estimates of fatigue life for the car suspension arm using the four master curves are shown in Fig. 5 for plane stress and plane strain conditions. The predicted lives using the four cases gave the following order with the shortest predicted life first.

(a) Lohr–Ellison parameter and biaxial fatigue data.
(b) Maximum shear strain parameter and biaxial fatigue data.
(c) Brown–Miller parameter and uniaxial fatigue data.
(d) Maximum principal strain and unixial fatigue data.

This was the sequence of predicted lives irrespective of the applied load range and also whether the plane stress or plane strain conditions were assumed to prevail.

5 Discussion

Fatigue design of service components should normally include factors about the manufacturing process, for example casting tolerances, surface roughness, residual stresses and other differences between similar components. Some of these factors probably contributed to the large scatter in the suspension arm fatigue results. Such factors were not included in the present analysis, however, and therefore the predicted lifetimes can only be assessed in a qualitative manner.

Of the fatigue life estimates for the suspension arm there are two immediate observations. Firstly, the estimates using biaxial data were consistently safer than those using uniaxial data, and secondly, the maximum strain parameter

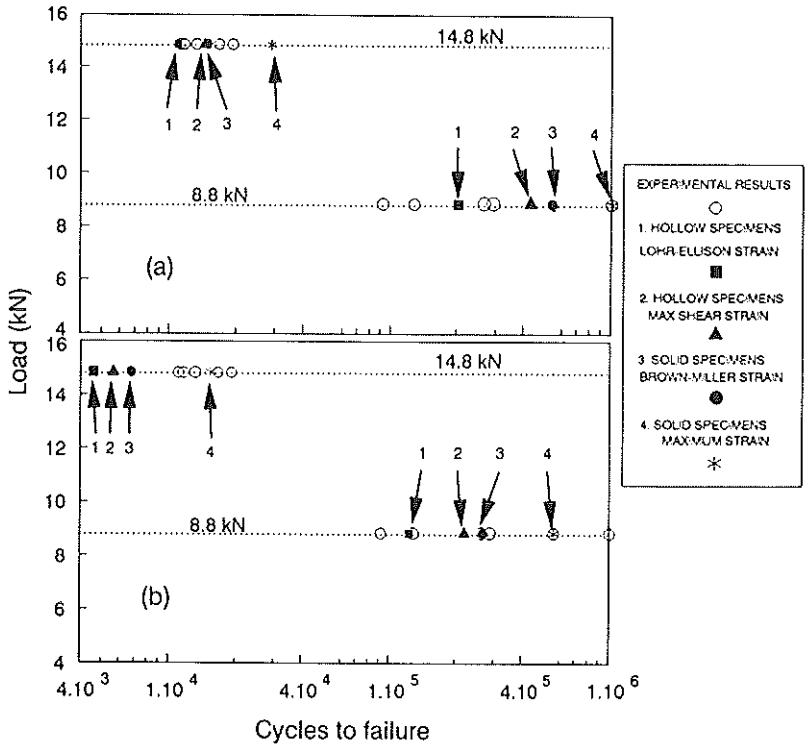

Fig 5 Estimated LCF lives for the suspension arm: (a) using plane-stress simulations; (b) using plane-strain simulations.

predictions were non-conservative compared to the results using the shear strain parameters. These two observations suggest that safer fatigue designs can be obtained using thin-walled biaxial data correlated with multiaxial strain parameters. Similar observations about conservative life estimates from thin-walled speciments subject to high strain torsion–tension tests were made by Miller and Chandler (**14**).

Finite-element simulations and strain gauge measurements have shown that at the suspension arm critical location a positive stress ratio (λ) existed on the surface. In the Brown–Miller terminology, Case B cracks would grow into the component wall (**7**). It was also assumed that Case B cracks dominated in the testing of the solid uniaxial specimens. For Case B cracks, the maximum shear strain plane is 45° through the thickness, and Brown–Miller and Lohr–Ellison theories are identical (9). For the thin-walled hollow specimens under a pure shear ($\phi = -1$) Case A was assumed to prevail (**10**). Thus for consistency with the Brown–Miller theory, the pure shear data was removed when the biaxial data was evaluated to obtain the master curve using the maximum shear strain, equation (4).

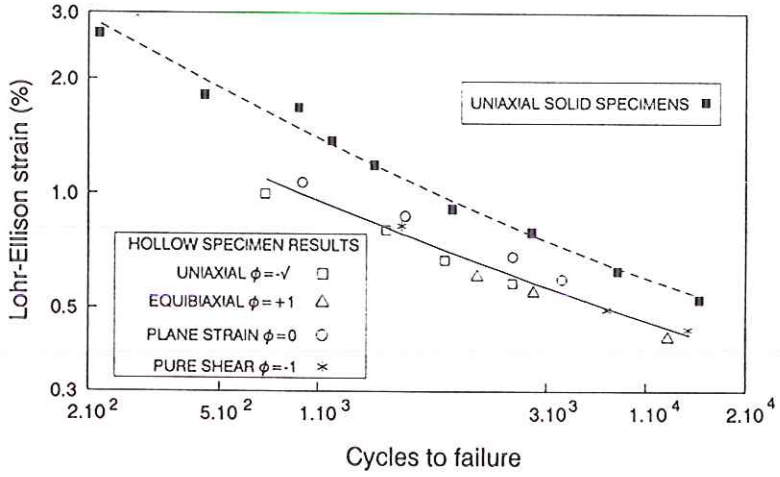

Fig 6 LCF life correlation of hollow and solid specimens using the Lohr–Ellison parameter.

The wall thickness of the biaxial specimens was about 1 mm (**10**) and it has been shown that for this geometry (**15**) there exists a stress and strain state which approximates to plane-stress, with almost no strain gradient across the specimen wall. The uniaxial specimens used an 8 mm diameter, and the LCF lives of the solid specimens were about three times greater than the LCF lives of the hollow specimens, when tested under the same conditions. This is shown in Fig. 6 where fatigue lives are correlated with the Lohr–Ellison strain parameter. This difference in lives is associated with a decreasing inward radial stress/strain gradient from the surface to the mid-section of the solid specimens. Similar observations of the difference in the fatigue lives between solid and thin-walled specimens were previously obtained from biaxial tests of other steels (**11, 14, 16**). Therefore, for improved fatigue estimates the influence of the strain gradient is required.

In the past, thickness stress modifications were introduced (**17**) to high cycle fatigue (HCF) results. To accommodate for the geometrical variation between the solid and thin-walled specimens in LCF, a simple analysis was developed which modifies the surface strain with a parameter based on the inward strain gradient.

The subsurface analysis evaluated an incremental damage in a critical path through the specimen thickness. This damage value is relative to the distance from the surface and used the simulated local strain gradient at finite distances under the surface. The damage values were then used to modify the lives corresponding to each incremental simulated strain employing a biaxial fatigue master curve. Finally the values of the modified subsurface incremental fatigue lives were summed up in a similar way to Miner's rule to give the total life to failure. The damage analysis is given in the Appendix.

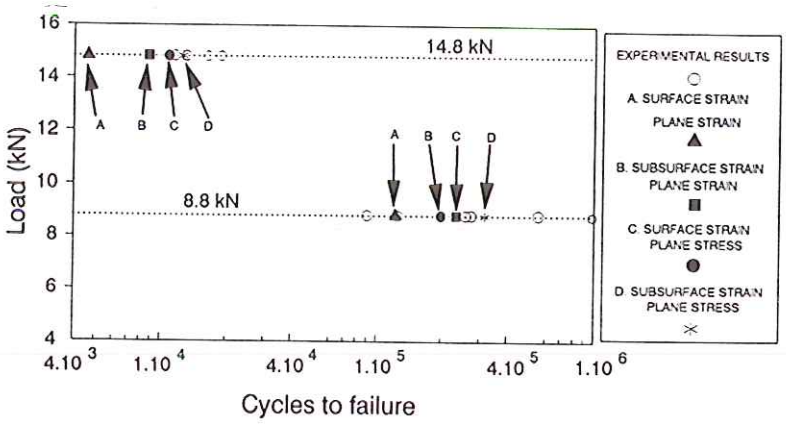

Fig 7 Estimated LCF lives using Lohr–Ellison parameter and subsurface analysis.

The subsurface analysis was used to calculate the suspension arm lives using the Lohr–Ellison theory. Figure 7 shows the estimated lives using plane stress and plane strain conditions. The predicted lives are less conservative than those obtained with the surface strain (Figs 5 and 6) and similar to those obtained using the solid specimens and the Brown–Miller parameter.

6 Concluding Comments

A high-strain, constant amplitude multiaxial fatigue life prediction procedure was applied to predict the fatigue lives of a car suspension arm subjected to cyclic loading. Two sets of experimental data were used for the life prediction, (a) from the biaxial fatigue of thin-walled specimens, and, (b) from the uniaxial fatigue of solid bar specimens. Simulated cyclic strains at a critical location were used together with multiaxial strain prediction theories to predict the lives.

At high cyclic loads conservative estimates of service component life were obtained using LCF data from thin-walled biaxial specimens, employing Brown–Miller and Lohr–Ellison multiaxial fatigue correlation. At the lower load range less conservative results were obtained. The predictions of the component fatigue life from uniaxial solid specimens were non-conservative, particularly when the biaxiality state was not included.

The shorter estimated life from the thin-walled biaxial fatigue data, as compared with the solid specimen fatigue data, was attributed to the geometrical differences and propagation of fatigue damage through the component thickness.

Acknowledgements

We acknowledge the support of this work by the Rover Group through the Brite JCR programme and the kind permission to use their experimental results.

References

(1) DOWLING, N. E., BROSE, W. R. and WILSON, W. K. (1977), Notched shaft fatigue life predictions by the local strain approach, *Fatigue Under Complex Loading*, SAE Publications, 6, pp. 55–81.

(2) HURD, N. J. and IRVING, P. E. (1985) Smooth specimens fatigue lives and microcrack growth modes in torsion, *Multiaxial Fatigue*, **ASTM STP 853**, pp. 267–284.

(3) BROWN, M. W. and MILLER, K. J. (1982) Two decades of progress in the assessment of multiaxial low-cycle fatigue life, **ASTM STP 770**, pp. 482–499.

(4) HOFFMAN, M. and SEEGER, T. (1985) A generalised method for estimating multiaxial elastic-plastic notch stresses and strains Part 1: Theory, Part 2: Application and general discussion, *J Engng Mat and Tech*, **107**, pp. 250–260.

(5) TIPTON, S. M. and NELSON, D. V. (1985) Fatigue life predictions for a notched shaft in combined bending and torsion, *Multiaxial Fatigue*, **ASTM STP 853**, pp. 514–550.

(6) GARUD, Y. S. (1981) Multiaxial fatigue: a survey of the state of the art, *J. Test. Eval.* **9**, (3), pp. 165–178.

(7) BROWN, M. W. and MILLER, K. J. (1973) A theory for fatigue failure under multiaxial stress–strain conditions, *Proc. Inst. Mech. Engng.* **187**, pp. 745–755.

(8) KANDIL, F. A., BROWN, M. W. and MILLER, K. J. (1982) Biaxial low cycle fatigue failure of 316 stainless steel at elevated temperature, *J. Metal Society*, **280**, pp. 203–209.

(9) LOHR, R. D. and ELLISON, E. G. (1980) A simple theory for low cycle multiaxial fatigue, *Fatigue Engng Mater Struct*, **3**, pp. 1–17.

(10) SHATIL, G., SMITH, D. J. and ELLISON, E. G. (1994) High-strain biaxial fatigue of a structural steel, *Fatigue Engng Mater Struct*, **17**, (2), pp. 159–170.

(11) FASH, J. W., HURD, N. J., HUA, C. T. and SOCIE, D. F. (1988) Damage development during multiaxial fatigue of unnotched and notched specimens, *Low Cycle Fatigue*, **ASTM STP 942**, pp. 874–898.

(12) SHATIL, G., ELLISON, E. G. and SMITH, D. J. (1995) Elastic-plastic behaviour and uniaxial low cycle fatigue life of notched specimens, *Fatigue Engng Mater Struct*, **18**, (2), pp. 235–245.

(13) DEVLUKIA, J. (1989) Rover Group, private communication.

(14) MILLER, K. J. and CHANDLER, D. C. (1969) High strain torsion fatigue of solid and tubular specimens, *Proc. I Mech Eng.*, **184**, (25), pp. 433–448.

(15) LOHR, R. D. and ELLISON, E. G. (1977) Biaxial high-strain fatigue testing of 1 CrMoV steel, *J. Struct. Anal.* **8**, pp. 168–172.

(16) JACQUELIN, B., HOURLIER, F. and PINEAU, A. (1983) Crack initiation under low-cycle multiaxial fatigue in type 316L stainless steel, *J Press Vessel Tech*, **105**, pp. 138–143.

(17) FLAVENOT, J. F. and SKALLI, N. (1989) A critical depth criterion for the evaluation of long-life fatigue strength under multiaxial loading and stress gradient, *Biaxial and Multiaxial Fatigue*, EGF 3, (Edited by M. W. Brown and K. J. Miller), MEP Publications, pp. 355–365.

Appendix

Subsurface analysis

In the proposed subsurfaces damage analysis D_n is defined as the incremental through thickness damage and N_{fn} as the cycles to failure related to a particular increment. Applying Miner's rule to the damage model assume that

$$D_n = \frac{N_n}{N_{fn}} \tag{A1}$$

where D_n is the damage for a particular equivalent strain calculated from the master curve of equations (3) and (4), and

$$\Sigma D_n = 1 \quad \text{and also,} \quad N_n = D_n N_{fn} \tag{A2}$$

The input strain to calculate N_n for a particular increment is calculated as follows

$$\bar{\varepsilon}_n = \frac{\varepsilon_i + \varepsilon_{i-1}}{2} \tag{A3}$$

where: $\bar{\varepsilon}_n$ = average incremental strain; n = increment number; $n = 1$ in the surface increment; i = increment edges; $i = 0$ at the surface ($i = n - 1$).
The incremental damage parameter D_n, which is a nondimensional strain gradient value, is given as

$$D_n = \frac{\varepsilon_{i-1} - \varepsilon_i}{\Delta\varepsilon} \tag{A4}$$

where: $\Delta\varepsilon$ = total strain gradient at 1 mm distance which is the wall thickness of the biaxial specimens.

Next, the relative distance from the surface of each strain increment is taken into account by introducing an 'effective incremental damage parameter', D_n^*, given as

$$D_n^* = D_n \left\{ 1 - \left(\sum_{m=1}^{m=n-1} D_n^* \right) \right\} \tag{A5}$$

This means that each incremental damage is modified by a value that is relative to its surface position. After calculating the modified incremental damage, the total life to failure is summed in a similar way to Miner's rule

$$N_{f*} = \sum_{1}^{n} (N_{fn} D_n^*) \tag{A6}$$